Available online at www.sciencedirect.com
ScienceDirect
Journal of Computational Physics 226 (2007) 398–413
JOURNAL OF COMPUTATIONAL PHYSICS
www.elsevier.com/locate/jcp

An isochoric domain deformation method for computing steady free surface flows with conserved volumes

Xueying Xie [a], Lawrence C. Musson [c], Matteo Pasquali [a,b,*]

[a] *Department of Chemical & Biomolecular Engineering, Computer and Information Technology Institute, Rice University, MS 362, 6100 Main Street, Houston, TX 77005, USA*
[b] *Department of Chemistry, Carbon Nanotechnology Laboratory, The Smalley Institute for Nanoscale Science & Technology, Rice University, USA*
[c] *Sandia National Laboratories, P.O. Box 5800 MS-0316, Albuquerque, NM 87185, USA*

Received 31 July 2006; received in revised form 10 April 2007; accepted 13 April 2007
Available online 13 May 2007

Abstract

The domain deformation method has been applied successfully to steady state free surface flows where the volume of the flow domain is unknown [V.F. de Almeida, Gas–liquid counterflow through constricted passages, Ph.D. thesis, University of Minnesota, Minneapolis, MN 1995; P.A. Sackinger, P.R. Schunk, R.R. Rao, A Newton–Raphson pseudo-solid domain mapping technique for free and moving boundary problems: a finite element implementation, J. Comput. Phys. 125 (1996) 83–103; L.C. Musson, Two-layer slot coating, Ph.D. thesis, University of Minnesota, Minneapolis, MN 2001]; however, this method does not handle effectively problems where the volume of the flow domain is known *a priori*. This work extends the original domain deformation method to a new isochoric domain deformation method to account for the volume conservation. Like in the original domain deformation method, the unknown shape of the flow domain is mapped onto a reference domain by using the equations of an elastic pseudo-solid; the difference with the original method is that this pseudo-solid is considered incompressible. Because of the incompressibility, the pseudo-pressure of the mapping appears as a Lagrange multiplier in the equations, and it is determined only up to an arbitrary uniform datum. By analyzing the coupled fluid flow-mapping problem, we show that, in the finite-element setting, such pressure datum can be specified by replacing one continuity equation in the fluid domain.

Keywords: Domain deformation method; Free surface flows; Free-boundary problems; Isochoric mapping method; Finite element method

1. Introduction

Flows with free surfaces have movable boundaries whose shapes are achieved by a balance of all the forces evident in viscous flow plus capillarity—the action of surface tension in a curved interface. In most free surface

* Corresponding author. Address: Department of Chemical & Biomolecular Engineering, Computer and Information Technology Institute, Rice University, MS 362, 6100 Main Street, Houston, TX 77005, USA. Tel.: +1 713 348 5830.
E-mail address: mp@rice.edu (M. Pasquali).

0021-9991/$ - see front matter
doi:10.1016/j.jcp.2007.04.028

flows, for example, slot coating and polymer extrusion flow, both the shape and the volume of the flow domain are unknown *a priori*. However, the volume of the fluid in the domain is occasionally known *a priori*. For example, a neutrally buoyant immiscible drop suspended in a flowing fluid can deform its shape, but the volume of the droplet is conserved.

Previously, several methods for handling steady free surface problems have been developed, in particular using so-called elliptic mesh generation [4] and domain deformation [2,5]. These methods have been successful in describing 2D free surface problems [1,3,6–8]. In addition, the domain deformation method has been applied successfully to 3D Newtonian free surface problems [9] and 3D viscoelastic free surface flows [10,11]. These methods compute the shape of the free surfaces together with the flow equations by mapping the physical (flow) domain onto a reference domain; however, the mapping does not preserve the domain volume. Whereas free surface flows with open boundaries are solvable by a suitable prescription of open-flow boundary conditions, models of closed flows with moving boundaries are under-determined without a mathematical constraint that prescribes the volume that the liquid occupies; one example is a deforming droplet suspended in a shearing flow. Although a new method has been presented recently to preserve the mapping volume locally in an unsteady flow [12], no such method is currently available for steady flows.

This paper extends the original domain deformation method to preserve the volume of the reference domain in a steady flow, so that the volume of the physical domain is equal to the volume of the reference domain. The finite element method is then applied to solve the problem equations and to determine the shape of the flow domain. The new method is called the isochoric domain deformation method. In this new method, the mesh is treated as an incompressible elastic pseudo-solid, so that the physical domain is related to a reference domain through an isochoric mapping. Here, the isochoric domain deformation method is evaluated by solving volume-conserved steady free surface problems with Newtonian liquids; the method is universally applicable to non-Newtonian fluids.

Section 2 presents the mathematical formulation and the solution method. Sections 3–5 present 2D and 3D test cases for validating the isochoric domain deformation method. Section 6 tests the effectiveness of the method in handling large domain deformations. Finally, Section 7 summarizes the results and assesses the potential of the isochoric domain deformation method.

2. Mathematical formulation and solution method

Steady, free surface flows modeled by the isochoric domain deformation method are described by the coupled domain volume conservation equation, domain mapping equation, mass conservation equation, and momentum conservation equation. These equations are coupled and simultaneously yield domain shape and flow field. The problem equations are

$$0 = \det \mathbf{F}^{\mathrm{d}} - 1 \tag{1}$$

$$0 = \nabla \cdot \mathbf{T}^{\mathrm{e}} \tag{2}$$

$$0 = \nabla \cdot \mathbf{v} \tag{3}$$

$$0 = \rho \mathbf{v} \cdot \nabla \mathbf{v} - \nabla \cdot \mathbf{T} - \nabla \Theta \tag{4}$$

where det indicates the determinant of a tensor, $\mathbf{F}^{\mathrm{d}}$ is the domain mapping deformation gradient tensor, ∇ is the gradient vector in space, $\mathbf{T}^{\mathrm{e}}$ is the stress tensor of the elastic pseudo-solid, $\mathbf{v}$ is the velocity, ρ is the fluid density, $\mathbf{T} = -p\mathbf{I} + \mu(\nabla \mathbf{v} + \nabla \mathbf{v}^{\mathrm{T}})$ is the total stress tensor of the fluid, p is the pressure, μ is the fluid viscosity, $\mathbf{I}$ is the identity tensor, superscript T denotes the transpose, and Θ is the potential body force per unit volume.

Eq. (1) expresses volume conservation for the pseudo-solid. Eq. (2) is the pseudo-solid momentum equation and it is also called mapping equation in this study. These two equations describe an incompressible elastic pseudo-solid, i.e. the isochoric mapping. Eqs. (3) and (4) are fluid mass conservation equation and fluid momentum equation; they describe Newtonian fluid flow.

2.1. Isochoric domain deformation method

The isochoric domain deformation method treats the mesh as an incompressible elastic pseudo-solid and computes the mapping by solving the equilibrium equations of such pseudo-solid. Refs. [3,5,10,11] detail

the original domain deformation method. The isochoric domain deformation method follows a similar construction, except that a volume conservation constraint (Eq. (1)) is introduced and the elastic pseudo-solid constitutive equations are different.

Fig. 1 shows the elastic body mapping from the reference domain Ω_0 to the physical domain Ω

$$\mathbf{x} = \chi(\mathbf{x_0}) \tag{5}$$

where $\mathbf{x}$ is a point in Ω that corresponds to point $\mathbf{x}_0$ in Ω_0. An infinitesimal filament $\mathrm{d}\mathbf{x}_0$ at $\mathbf{x}_0$ deforms to $\mathrm{d}\mathbf{x}$ at $\mathbf{x}$ according to

$$\mathrm{d}\mathbf{x} = \mathbf{F}^{\mathrm{d}} \cdot \mathrm{d}\mathbf{x}_0; \quad \mathrm{d}x_i = F^{\mathrm{d}}_{ij}\,\mathrm{d}x_{0j} \tag{6}$$

where $\mathbf{F}^{\mathrm{d}}$ is called the domain mapping deformation gradient, and it is given by

$$\mathbf{F}^{\mathrm{d}} = (\partial\mathbf{x}/\partial\mathbf{x}_0)^{\mathrm{T}}; \quad F^{\mathrm{d}}_{ij} = \frac{\partial x_i}{\partial x_{0j}} \tag{7}$$

$\mathbf{F}^{\mathrm{d}}$ includes information of local deformation and rotation. Because rigid body rotation has no effect on equilibrium of solid, a new variable $\mathbf{B}$, the left Cauchy–Green strain tensor—also called the Finger tensor, is introduced to eliminate the rigid body rotation component by multiplying $\mathbf{F}^{\mathrm{d}}$ with its transpose,

$$\mathbf{B} = \mathbf{F}^{\mathrm{d}} \cdot \mathbf{F}^{\mathrm{d}^{\mathrm{T}}}; \quad B_{ij} = \frac{\partial x_i}{\partial x_{0k}} \frac{\partial x_j}{\partial x_{0k}} \tag{8}$$

$\mathbf{B}$ is positive definite and symmetric by construction.

In a domain mapping, there are two methods to conserve domain volume. The first method is to set

$$\int_{\Omega} \det \mathbf{F}^{\mathrm{d}}\,\mathrm{d}\Omega - V_0 = 0 \tag{9}$$

where V_0 is the reference domain volume. This method gives only one extra equation, but couples all the elements in this flow domain, thereby giving a full row in the Jacobian matrix that is used in Newton's non-linear equation solution method. Having such a full row is undesirable for parallel solvers because it requires extra inter-processor communication. The second method is to set

$$\det \mathbf{F}^{\mathrm{d}} - 1 = 0 \tag{10}$$

This method gives extra equations in each element, but only gives extra terms in the diagonal block of the Jacobian matrix, which is favorable for parallel solvers; thus, this study develops the second method.

The momentum-conservation equation of the pseudo-solid is

$$\nabla \cdot \mathbf{T}^{\mathrm{e}} = 0 \tag{11}$$

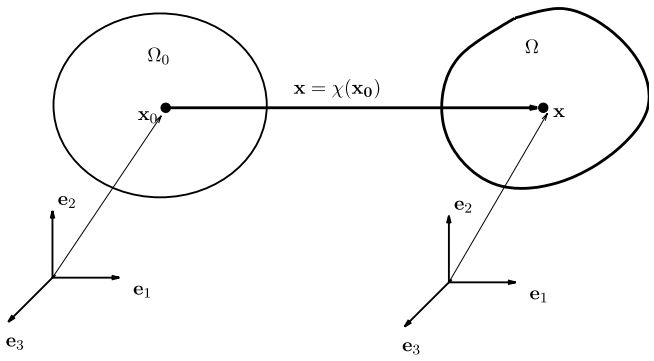

Fig. 1. Mapping between a reference domain Ω_0 and a physical domain Ω. χ is a mapping function that maps position $\mathbf{x}_0$ in Ω_0 to position $\mathbf{x}$ in Ω, and this mapping is a one-to-one mapping.

The momentum-conservation equation and the volume conservation equation forms a complete set to compute the deformation of an incompressible solid.

The constitutive equation of an incompressible pseudo-solid is [13]:

$$\mathbf{T}^{e} = -\pi\mathbf{I} + 2\mathbf{B}\cdot\frac{\partial w}{\partial \mathbf{B}} \tag{12}$$

where π is an arbitrary isotropic pressure of the pseudo-solid and it is called mapping pseudo-pressure hereafter; w is the stored energy depending on material model and deformation and it has a form of $w = f(\mathrm{I}_{\mathbf{B}}, \mathrm{II}_{\mathbf{B}}, \mathrm{III}_{\mathbf{B}})$, where $\mathrm{I}_{\mathbf{B}}, \mathrm{II}_{\mathbf{B}}, \mathrm{III}_{\mathbf{B}}$ are the first, second, and third invariants of $\mathbf{B}$. A discussion of the relative merits of various choices of stored energy functions can be found in Ref. [3]. For an incompressible elastic pseudo-solid, $\mathrm{III}_{\mathbf{B}} = (\det \mathbf{F}^{d})^2 = 1$; thus, $w = f(\mathrm{I}_{\mathbf{B}}, \mathrm{II}_{\mathbf{B}})$. Here an incompressible neo-Hookean elastic solid is chosen for simplicity and without loss of generality; its stored energy is $w = \frac{\beta_0}{2}(\mathrm{I}_{\mathbf{B}} - 3)$. Therefore, the elastic constitutive equation (Eq. (12)) can be rewritten as

$$\mathbf{T}^{e} = -\pi\mathbf{I} + \beta_0\mathbf{B} \tag{13}$$

where β_0 is a constant parameter related with solid shear modulus; $\beta_0 = 1$ is set in this study—a function $\beta(\mathbf{x})$ would easily yield an adaptive mesh.

The reference domain from which the mesh is deformed is completely arbitrary. In a first calculation, usually the initial guess of the domain shape and the mesh inscribed thereupon is used as the reference domain. In practice, solutions to free-boundary problems are rarely found unless, among other things, the initial guess is "relatively close" to the solution, and so mesh strains are not overly large. Thus convergence difficulties of the non-linear domain deformation equations are alleviated. Because one steady-state solution is of limited practical value, usually families of steady states are sought at wide ranges of operating and physical parameters most often by arc-length continuation techniques [14–16]. Again, because the reference state is arbitrary–and is thus a choice, the final configuration of the mesh at one steady state serves as the reference state for the succeeding state on the solution path. Thus, relative strains between consecutive continuation steps are always kept modest, whereas overall strains can be arbitrarily large (see Section 6). It should be noted, however, that the relative strains are not so modest as to render the quadratic strain measure equivalent to an infinitesimal one.

2.2. Free surface boundary conditions

The equations must be solved together with appropriate boundary conditions. Special care has to be taken on free surface for both the fluid flow momentum equation and pseudo-solid momentum equation, i.e. the mesh mapping equation. Fig. 2 shows the physical boundary conditions on free surfaces, where $\mathbf{n}_1$ and $\mathbf{n}_2$ are unit normal vectors on the surface of fluid 1 and fluid 2 domains, $\mathbf{T}_1$ and $\mathbf{T}_2$ are the total stress tensors in fluid 1 and fluid 2, respectively, ∇_{II} is the surface gradient which represents $(\mathbf{I} - \mathbf{nn})\cdot\nabla$, and $\mathbf{\Pi}$ is the surface stress with a tensor value of $\gamma(\mathbf{I}\text{-}\mathbf{nn})$ when the surface is a simple liquid–liquid or liquid–gas interface, $\mathbf{n}$ can be either $\mathbf{n}_1$ or $\mathbf{n}_2$ and γ is the surface tension. At the liquid free surface/interface, the physical boundary conditions show that dynamic equilibrium is

$$\mathbf{n}_1\cdot\mathbf{T}_1 + \mathbf{n}_2\cdot\mathbf{T}_2 = \nabla_{\mathrm{II}}\cdot\mathbf{\Pi} \tag{14}$$

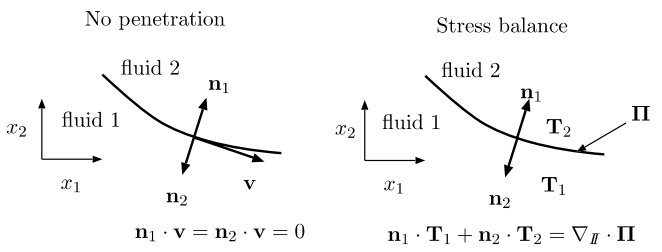

Fig. 2. Physical boundary conditions on free surface.

Eq. (14) is imposed naturally as fluid flow momentum equation boundary condition, i.e., through the weighted residual integral – the weak form in Galerkin's method – of the traction $\mathbf{n}\cdot\mathbf{T}$ at boundary Γ as

$$\int_\Gamma \psi^\alpha_{\mathbf{m}} \underbrace{\mathbf{n}_1\cdot\mathbf{T}_1}_{\text{traction in fluid 1}} \,\mathrm{d}\Gamma + \int_\Gamma \psi^\alpha_{\mathbf{m}} \underbrace{\mathbf{n}_2\cdot\mathbf{T}_2}_{\text{traction in fluid 2}} \,\mathrm{d}\Gamma = \int_\Gamma \psi^\alpha_{\mathbf{m}}(\nabla_{\mathrm{II}}\cdot\mathbf{\Pi})\,\mathrm{d}\Gamma$$
$$= -\int_\Gamma \nabla_{\mathrm{II}}\psi^\alpha_{\mathbf{m}}\cdot\mathbf{\Pi}\,\mathrm{d}\Gamma + \int_\Lambda \psi^\alpha_{\mathbf{m}}\mathbf{n}_\Lambda\cdot\mathbf{\Pi}\,\mathrm{d}\Lambda \tag{15}$$

where Λ is the boundary of boundary Γ (in 3D, Γ is a surface, Λ is a curve), $\mathbf{n}_\Lambda$ is outward unit normal vector of Λ and it is tangent to Γ at the same time, and $\psi^\alpha_{\mathbf{m}}$ is the weighting function α for the momentum equation ($\mathbf{m}$). In a free surface problem with only one liquid domain, $\mathbf{n}_2\cdot\mathbf{T}_2 = \mathbf{n}_1 p_{\mathrm{a}}$ with p_{a} the ambient pressure, the traction jump boundary condition becomes

$$\int_\Gamma \psi^\alpha_{\mathbf{m}} \underbrace{\mathbf{n}\cdot\mathbf{T}}_{\text{traction}} \,\mathrm{d}\Gamma = -\int_\Gamma \psi^\alpha_{\mathbf{m}}\mathbf{n}p_{\mathrm{a}} - \int_\Gamma \nabla_{\mathrm{II}}\psi^\alpha_{\mathbf{m}}\cdot\mathbf{\Pi}\,\mathrm{d}\Gamma + \int_\Lambda \psi^\alpha_{\mathbf{m}}\mathbf{n}_\Lambda\cdot\mathbf{\Pi}\,\mathrm{d}\Lambda \tag{16}$$

If it is a 2D problem, then the surface stress term in Eq. (15) is

$$\int_\Gamma \psi^\alpha_{\mathbf{m}}\nabla_{\mathrm{II}}\cdot\mathbf{\Pi}\,\mathrm{d}\Gamma = -\int_\Gamma \frac{\mathrm{d}\psi^\alpha_{\mathbf{m}}}{\mathrm{d}s}\mathbf{t}\cdot\mathbf{\Pi}\,\mathrm{d}\Gamma + \psi^\alpha_{\mathbf{m}}\mathbf{n}_\Lambda\cdot\mathbf{\Pi}\big|_a^b = -\int_\Gamma \frac{\mathrm{d}\psi^\alpha_{\mathbf{m}}}{\mathrm{d}s}\mathbf{t}\cdot\mathbf{\Pi}\,\mathrm{d}\Gamma + \psi^\alpha_{\mathbf{m}}(\mathbf{t}\cdot\mathbf{\Pi})_b - \psi^\alpha_{\mathbf{m}}(\mathbf{t}\cdot\mathbf{\Pi})_a \tag{17}$$

where $\mathbf{t}$ is the tangent to Γ, s is the path of the boundary line, a and b are the starting and the ending points of the boundary curve.

Imposing boundary conditions on the momentum equations of the pseudo-solid at the free surface is challenging because manipulating free surface characteristics on a 3D surface is difficult, especially on an unstructured mesh. A complete set of boundary conditions on the momentum equations requires three equations on a 3D surface; one component is normal to the surface and two are tangential to it and are usually orthogonal to one another. The normal component boundary condition is dictated by the physics whereas the tangential component equations can be chosen for computational convenience. The tangential equations are derived in such a way that material points of the pseudo-solid, represented by mesh nodes, form elements near the surface that are devoid of excessive skewness or aspect ratio.

The free surface is a streamline in 2D or surface in 3D, so there is no velocity component normal to it as shown in Fig. 2, i.e., $\mathbf{n}\cdot\mathbf{v} = 0$; this is called the kinematic boundary condition and it is applied in the normal direction as an essential boundary condition.

In the tangent directions, element nodes should move freely so as to achieve a desirable mesh quality. This is done by requiring the pseudo-solid surface to be free of shear stress, viz $\mathbf{t}_i\mathbf{n} : \mathbf{T}^{\mathrm{e}} = 0$, where $i = 1, 2$ in 3D flows and $\mathbf{t}_1$ and $\mathbf{t}_2$ are two orthogonal tangent vectors. Imposing this boundary condition on a boundary where one tangent vector is aligned with one coordinate direction is straightforward because the contribution of this term to the weighted residual is zero. Imposing this condition on a boundary which is arbitrarily oriented with respect to the coordinate system, e.g. a free surface, is more complicated. This condition can be applied either essentially or naturally in 2D flows [1–3]; in 3D flows it is applied naturally due to the difficulties in manipulating surface normal and tangent vectors and their derivatives. In a 3D problem, the mapping equations are projected onto two tangent directions; then the zero shear stress condition is imposed naturally. In general, the rotation can be done before or after integration of the volumetric terms of the equations; for simplicity, here the equations are rotated after integration as done in Ref. [9]. The residuals corresponding to $\mathbf{t}_1$ and $\mathbf{t}_2$ after rotation are

$$r^{\mathbf{x},\alpha}_{\mathbf{t}_1} = \mathbf{t}_1\cdot\mathbf{r}^{\mathbf{x},\alpha} \tag{18}$$

$$r^{\mathbf{x},\alpha}_{\mathbf{t}_2} = \mathbf{t}_2\cdot\mathbf{r}^{\mathbf{x},\alpha} \tag{19}$$

where $\mathbf{r}^{\mathbf{x},\alpha}$ is the mapping weighted residual equation associated with the mapping weighting function $\varphi^\alpha_{\mathbf{x}}$; the corresponding Jacobian matrix includes two contributions: (1) the derivatives of the vector residual projected onto the tangent directions and (2) the derivatives of the tangent vectors multiplied by the residuals. Computations reported below show that the quadratic convergence of Newton's iteration is preserved with this

rotation strategy. In 3D, there are countless tangent directions. Unit tangent vectors are usually different when they are calculated in different elements; however, the unit normal vectors are unique within numerical precision. In order to obtain two unit orthogonal tangent vectors consistent for each node shared by elements, the tangent vectors are computed globally. For each node on free boundary, the first unit tangent vector is calculated by

$$\mathbf{t}_1 = \frac{(\mathbf{I} - \mathbf{nn}) \cdot \mathbf{s}}{\|(\mathbf{I} - \mathbf{nn}) \cdot \mathbf{s}\|} \tag{20}$$

where $\mathbf{s}$ is an arbitrary seed vector [9], chosen to be sufficiently different from $\mathbf{n}$ to avoid a vanishing product in the projection. The second unit tangent vector is calculated from the unit normal vector and the first unit tangent vector

$$\mathbf{t}_2 = \mathbf{n} \times \mathbf{t}_1 \tag{21}$$

At edges when two or more surfaces meet, special care must be taken for the boundary conditions. If different boundary conditions are prescribed on the surfaces meeting at one edge or corner, one of them must be kept and the others must be discarded. If the node location is specified on any of the surfaces, this condition is imposed preferentially. Alternatively, the kinematic boundary condition is imposed. If neither of these two conditions is prescribed, the node distribution boundary condition is imposed.

2.3. Coupling of fluid and elastic pseudo-solid

To solve the free surface flow equations involves computing a fluid flow field and a mesh. The equations for liquid and pseudo-solid are coupled to solve the problem simultaneously; the coupling is strong when surface tension is high—more precisely, when the capillary number $\mathrm{Ca} \equiv \mu v/\gamma$ is low. The kinematic boundary condition, $\mathbf{n} \cdot \mathbf{v} = 0$, couples solid and liquid because this fluid flow condition is imposed as a boundary condition on the mapping equation; this coupling exists regardless of the method used to compute the mapping. Most importantly, in the isochoric domain deformation method, one continuity equation in one location is replaced by an equation that sets the mapping pseudo-pressure π a constant reference value; the reason is explained below.

When computing the deformation of an incompressible pseudo-solid, the variable π is a Lagrange multiplier and it only appears in a gradient form in the pseudo-solid momentum equation; thus, π is specified up to a reference value—much like the pressure in an incompressible liquid or solid. The reference value can be introduced either by a normal elastic stress boundary condition or by setting a value of π at one location. However, on known boundaries, the boundary shape must be imposed as boundary condition; on free boundaries, the kinematic boundary condition is imposed. Therefore, a normal elastic pseudo-stress cannot be imposed through the boundary, and an arbitrary value of π, i.e., $\pi = \pi_0$, has to be set at one interior location. This apparent paradox can be resolved by examining the continuity equation and kinematic boundary condition in the flow domain.

In free surface flows with conserved domain volumes, there are no inflow or outflow surfaces; thus, the normal velocity on all boundaries is zero. On each free boundary, $\mathbf{n} \cdot \mathbf{v} = 0$ is imposed explicitly as essential boundary condition on the elastic pseudo-solid equilibrium equation. On all the other boundaries, $\mathbf{n} \cdot \mathbf{v} = 0$ is generally imposed implicitly through Dirichlet boundary conditions, $\mathbf{v} = \mathbf{f}(\mathbf{x})$, where $\mathbf{v}$ has zero value in normal direction. By the divergence theorem [17],

$$\int_{\Omega} \nabla \cdot \mathbf{v} \, \mathrm{d}\Omega = \int_{\Gamma} \mathbf{n} \cdot \mathbf{v} \, \mathrm{d}\Gamma \tag{22}$$

Therefore, the zero normal velocity on the whole boundaries and the mass conservation equation in the whole domain are linearly dependent. One of the weighted residuals of the continuity equation must be replaced to generate a set of linearly independent problem equations.

The mapping pseudo-pressure reference value equation $\pi = \pi_0$ is introduced in place of this superfluous continuity residual. Replacing one continuity residual equation by setting a reference value of π not only removes one linearly dependent equation in the fluid flow domain, but also closes the incompressible solid

equation set. Thus, this replacement closely couples solid and fluid to form a closed equation set, and it is a key advantage of the isochoric domain deformation method.

2.4. Solution method

The Galerkin finite element method is used to reduce the partial differential equations of the problem to algebraic equations [11]. The problem equations are non-linear and fully coupled. Newton's method is used to linearize the equations, which yields a large scale linear algebraic system $\mathbf{J}\Delta\mathbf{x} = -\mathbf{R}$, where $\mathbf{J}$ is the Jacobian matrix, $\Delta\mathbf{x}$ is called the Newton update, and $\mathbf{R}$ is the residual vector. The Jacobian matrix is computed analytically so that the iterative solver converges quadratically. In each Newton iteration, a direct frontal solver with full pivoting [18] solves the linear algebraic equations. Convergence is declared when both $\|\Delta\mathbf{x}\|_2$ and $\|\mathbf{R}\|_2$ are less than 10^{-6}, where $\|\cdot\|_2$ denotes the Euclidean norm. Typically, four to six Newton iterations are necessary for convergence.

3. Computation of a 2D slit with a free surface

The isochoric domain deformation method is applied to compute a 2D free surface between two static parallel plates. The slit is filled with a liquid of prescribed volume V_0. As shown in Fig. 3, the meniscus in the slit is not flat. The distance between the plates is $w = 1$ and the volume per unit breadth of the liquid between the plates is $V_0 = 4w^2$. The problem is mapped onto a reference rectangular domain with height $h = 4w$ and width w. In this static situation, a dimensionless number, Bond number, $Bo = \rho g w^2/\gamma$ is defined to express the ratio of gravitational forces to surface tension forces; here g is acceleration due to gravity and γ is the surface tension. In this study, Bo is fixed at 0.5 and the contact angle is set to $\theta = 60^{\circ}$.

The boundary conditions for this case are: (1) on boundary 1, the essential boundary conditions are $\mathbf{x} = \mathbf{x}_0$ and $\mathbf{v} = \mathbf{0}$; (2) on boundaries 2 and 3, the mesh adheres to the equation of the lines $x_i = x_{i0}$ $(i = 2, 3)$ respectively and moves freely on the line by following the tangent boundary condition $\mathbf{tn} : \mathbf{T}^{\mathrm{e}} = 0$, and $\mathbf{v} = \mathbf{0}$; (3) on boundary 4, free surface boundary conditions are imposed, i.e., $\mathbf{n} \cdot \mathbf{v} = 0$, $\mathbf{tn} : \mathbf{T}^{\mathrm{e}} = 0$, and $\mathbf{n} \cdot \mathbf{T} = -\mathbf{n}p_{\mathrm{a}} + \nabla_{\mathrm{II}} \cdot \mathbf{\Pi}$.

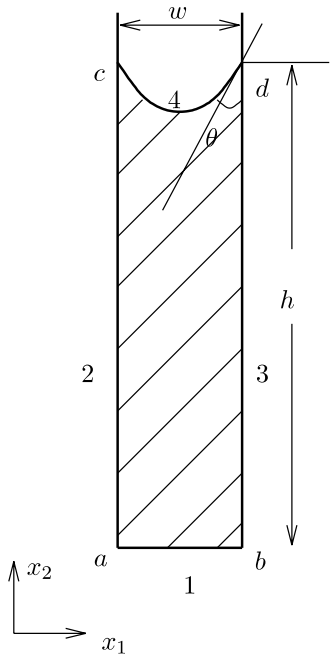

Fig. 3. Schematic of a constant volume of liquid between two parallel plates with a meniscus. The numbers 1–4 denote the boundaries, and the letters a–d denote the intersection corners.

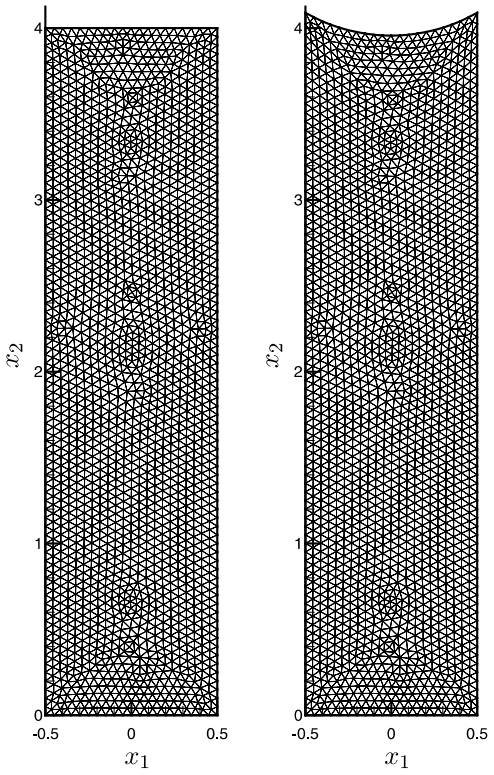

Fig. 4. Reference and deformed physical meshes of the 2D slit between two parallel plates with a conserved volume of fluid. Left: reference mesh; right: computed physical mesh.

Boundary conditions for the intersections are: (1) at the intersections a and b, boundary conditions of the boundary 1 are imposed; (2) at the intersections c and d, fluid momentum boundary condition of boundaries 2–3 are imposed, but for the mesh equation, $x_1 = x_{10}$ and the contact angle $\theta = 60°$ of the meniscus with the wall are imposed. The contact angle boundary condition is imposed by specifying the normal vector direction at the intersections c and d on boundary 4.

The above boundary conditions indicate that $\mathbf{n} \cdot \mathbf{v} = 0$ on all the boundaries. However, $\mathbf{n} \cdot \mathbf{v} = 0$ on all the boundaries and the continuity equation $\nabla \cdot \mathbf{v} = 0$ in all the domain are linearly dependent according to the divergence theorem. As described in detail in Section 2.3, one mass conservation equation is replaced by equation $\pi = 0$ at the bottom left corner a.

The triangular mesh of the reference domain Ω_0 is shown in Fig. 4 (left). The reference domain has a flat top and its height is $h_0 = 4w$ so that the volume of the domain equals the volume of the liquid inside the slit. The mesh has 902 elements and 1905 nodes. The mesh and fluid equations are solved to obtain the final meniscus shape for the specified boundary conditions. Fig. 4 (right) shows the computed mesh.

Fig. 5 shows the shape of the free surface; the volume of fluid, which is $V_0 = 4w^2$ in the reference domain, is computed in the physical domain. The computed volume is 4.0001 w^2, which equals the reference volume V_0 to within 0.0025%, confirming that the volume is conserved.

Fig. 6 shows the contours of the liquid pressure p and mapping pseudo-pressure π. The contours show that π has a higher value in the middle of the free surface and a lower value at the corners. This is attributed to the distortion of the mesh elements in the middle and the stretch at the corners as shown in Fig. 4 (right).

4. Computation of a Newtonian drop deforming in a Newtonian shear flow

The deformation of a periodic suspension of drops in a shear flow with an immiscible fluid is calculated by applying the isochoric domain deformation method in the drop domain and original compressible domain

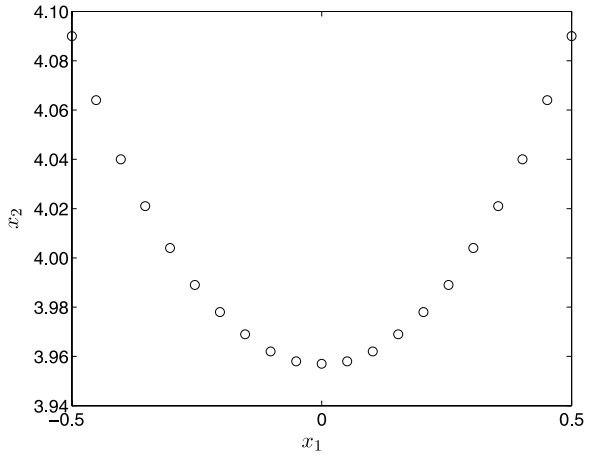

Fig. 5. Free surface shape in a slit (2D) with a conserved volume of fluid. The open circles denote the computed values.

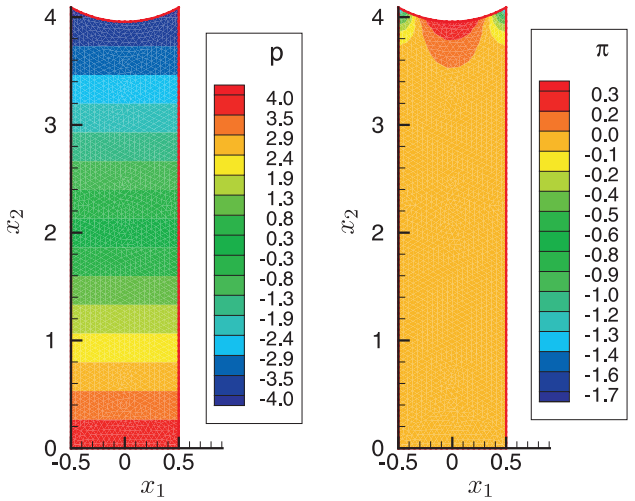

Fig. 6. Contours of the liquid pressure p (left) and mapping pseudo-pressure π (right) in the 2D slit with a conserved volume of fluid.

deformation method in the matrix domain. The schematic of the flow domain is shown in Fig. 7, with dimension $2H = 8R_0$ and $L = 8R_0$, where R_0 is the undeformed drop radius, $2H$ is the width between the top and the bottom boundary, and L is the length. The Reynolds number is $Re \equiv 2\rho U_0 R_0/\mu_m$, where μ_m is the viscosity of the external phase, and it is fixed at $Re = 0$. The viscosity ratio between the drop and the matrix fluid is fixed at $q = 1$. The characteristic shear rate is $\dot{\gamma}_c = U_0/H$; thus, the capillary number is $Ca \equiv \mu R_0(U_0/H)/\gamma$. The boundary conditions are: (1) the top boundary moves in the positive x_1 direction with a constant velocity U_0, i.e., $\mathbf{v} = U_0\mathbf{e}_1$, (2) the bottom boundary moves opposite to x_1 direction with a constant velocity U_0, i.e., $\mathbf{v} = -U_0\mathbf{e}_1$, (3) the flow field on the left and right open boundaries is periodic, and (4) the drop surface is a free interface. The kinematic boundary condition, $\mathbf{n} \cdot \mathbf{v} = 0$, is imposed as mesh boundary condition on the drop surface. By the divergence theorem [17], the kinematic boundary condition integrated over the whole drop surface is equivalent to the continuity equation $\nabla \cdot \mathbf{v} = 0$ integrated over the whole drop domain. Thus, the weighted continuity equation at one node in the drop domain must be replaced, in this case, by $\pi = 0$ to create a linearly independent set of weighted residuals. Because the problem is translationally invariant, the center location of the drop is specified so as to fix the location of the drop and create a closed set of equations.

With domain dimensions and viscosity ratio q fixed and boundary conditions set, the drop morphology depends only on capillary number for a Newtonian drop deforming in a Newtonian matrix. The drop

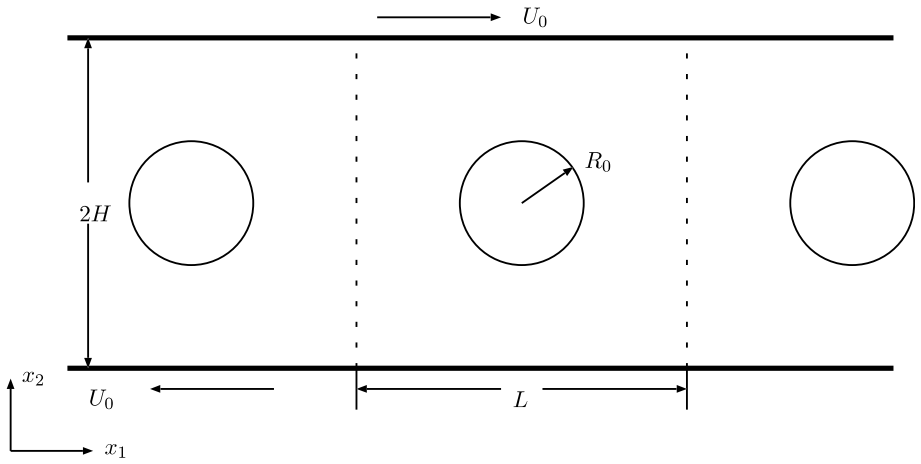

Fig. 7. Schematic of a periodic suspension of 2D drops in a channel flow. The domain of the computation is the middle domain with length L.

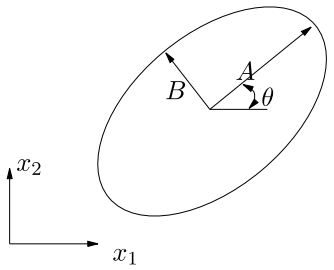

Fig. 8. Schematic of drop shape and orientation. A is the maximum radius, B is the minimum radius, and θ is the orientation angle between the maximum radius direction and the x_1-axis.

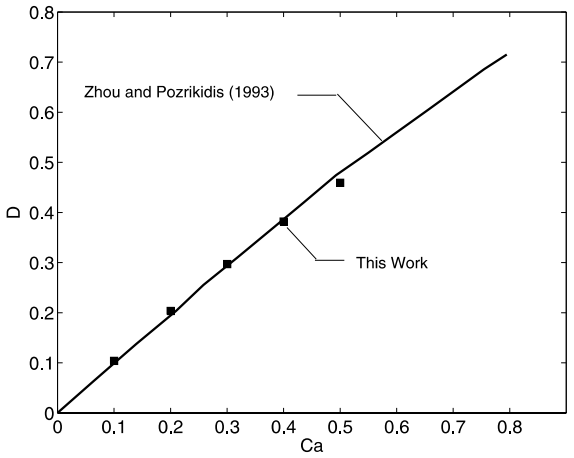

Fig. 9. D versus Ca for a 2D periodic Newtonian drop deforming in a Newtonian matrix; comparison of this work with Zhou and Pozrikidis [19].

morphology is represented by the deformation parameter D defined as $D = (A - B)/(A + B)$ and orientation angle θ, where A, B and θ are described by Fig. 8. For code validation, this test uses the same parameters and geometry as those of Ref. [19]. Fig. 9 shows the relationship between deformation parameter D and capillary

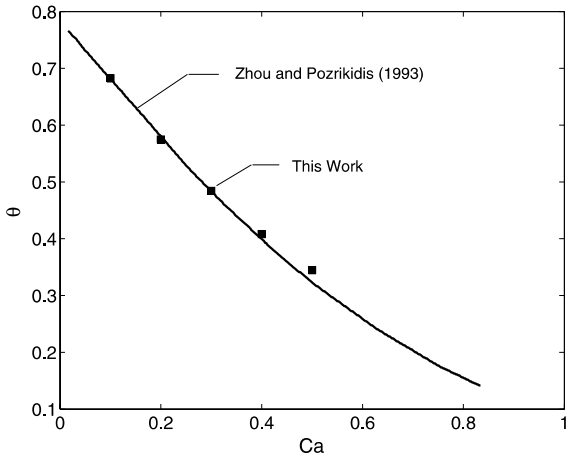

Fig. 10. θ versus Ca for a 2D periodic Newtonian drop deforming in a Newtonian matrix; comparison of this work with Zhou and Pozrikidis [19].

number Ca. Fig. 10 shows the drop orientations at different capillary numbers. In both figures, the data comparison to the results presented in [19] is excellent up to $Ca \approx 0.4$.

5. Computation of a 3D rotating bucket flow

The isochoric domain deformation method is applied to a 3D rotating bucket filled with a liquid volume of V_0 as shown in Fig. 11. The analytical free surface shape is available for validating the method. The radius of the bucket is R. The volume of the liquid is $V_0 = \bar{\pi}R^2H$ (here, $\bar{\pi}$ is Archimedes' constant; hereafter, $H \equiv R$). The bucket rotates in clock-wise direction at an angular speed ω under the influence of gravity (directed

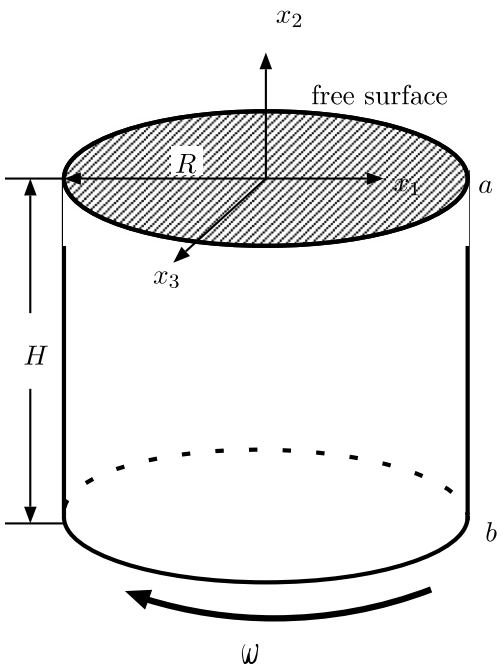

Fig. 11. Schematic of the rotating bucket flow. The top surface is a free surface and the other boundaries are solid walls.

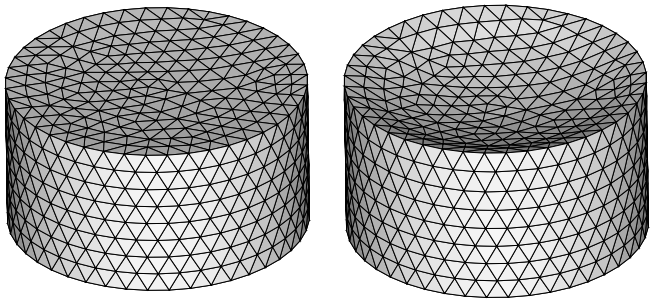

Fig. 12. Computed meshes in a rotating bucket flow with a constant volume at different Froude numbers. Left: $Fr = 0.1$; right: $Fr = 0.4$.

toward the bottom of the bucket, i.e., parallel to the axis of rotation). The Froude number, defined as the ratio of inertial to gravitational force, is set at $Fr \equiv R\omega^2/g = 0.1$ to 0.4.

The boundary conditions are: (1) on the bottom boundary, $\mathbf{x} = \mathbf{x}_0$, and the velocity of the liquid equals that of solid wall $\mathbf{v} = \mathbf{v}_w$, i.e., $v_1 = -x_3\omega$, $v_2 = 0$, and $v_3 = x_1\omega$; (2) on the side wall, the mesh can only move in the direction of the axis of rotation, i.e., $x_1 = x_{10}$, $x_3 = x_{30}$, and $\mathbf{tn} : \mathbf{T}^e = 0$, with $\mathbf{t}$ parallel to the x_2 direction, and the velocity of the liquid equals that of solid wall $\mathbf{v} = \mathbf{v}_w$, i.e., $v_1 = -x_3\omega, v_2 = 0, v_3 = x_1\omega$; (3) on the top surface, free surface boundary conditions are imposed, i.e., $\mathbf{n} \cdot \mathbf{v} = 0$, $\mathbf{t_1 n} : \mathbf{T}^e = 0$, $\mathbf{t_2 n} : \mathbf{T}^e = 0$, where $\mathbf{t_1}$ and $\mathbf{t_2}$ are two orthogonal unit tangent vectors, and force balance at free surface $\mathbf{n} \cdot \mathbf{T} = -\mathbf{n}p_a + \nabla_{II} \cdot \mathbf{\Pi}$. Boundary conditions at the intersections are: (1) at the intersection a, the boundary conditions on the bottom boundary are applied; (2) at the intersection b, the boundary condition from the free surface is applied to the mapping equations; the conditions $v_1 = -x_3\omega$, $v_3 = x_1\omega$, and $(\mathbf{n} \cdot \mathbf{T})_2 = (-\mathbf{n}p_a + \nabla_{II} \cdot \mathbf{\Pi})_2$ are imposed on the momentum equation.

The above boundary conditions prescribe that $\mathbf{n} \cdot \mathbf{v} = 0$ on all the boundaries. One mass conservation equation is replaced by equation $\pi = 0$.

The computation is performed on an tetrahedral mesh with 969 elements and 1674 nodes. At different Froude number, the computed mesh and velocity vectors are shown in Figs. 12 and 13, respectively. The free surface shape only depends on the Froude number, and the height from the bottom to the top free surface (circle a), which equals H_0 at static state, increases with Froude number. The analytical free surface shape is

$$x_2/R = \frac{1}{2}Fr\left(\frac{r}{R}\right)^2 - \frac{Fr}{4} + x_{20}/R \tag{23}$$

where x_2/R is the dimensionless free surface shape, x_{20} is the top surface location in the absence of rotation, and $r \equiv \sqrt{x_1^2 + x_3^2}$. The computed free surface shapes at $Fr = 0.1$ and $Fr = 0.4$ are plotted at the $x_3 = 0$ plane in Fig. 14 (left). The free surface deforms more as Froude number increases, but it always meets the static profile at radius $r^* = R/\sqrt{2}$ as expected. Fig. 14 (left) compares the computed free surface shapes with the analytical shapes. Fig. 14 (right) shows the relative error, which is calculated by dividing the difference between the analytical and numerical solutions by the total analytical deformation depth. The comparison shows that the

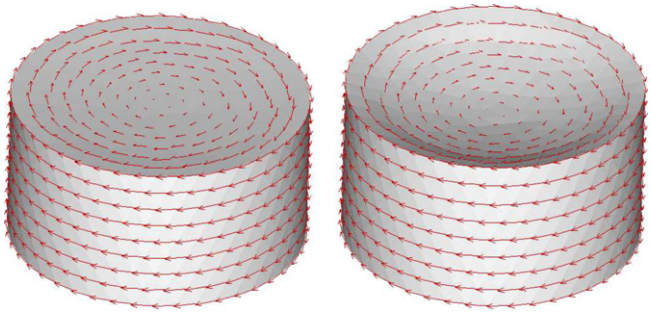

Fig. 13. Velocity vectors in a rotating bucket flow with a constant volume at different Froude numbers. Left: $Fr = 0.1$; right: $Fr = 0.4$.

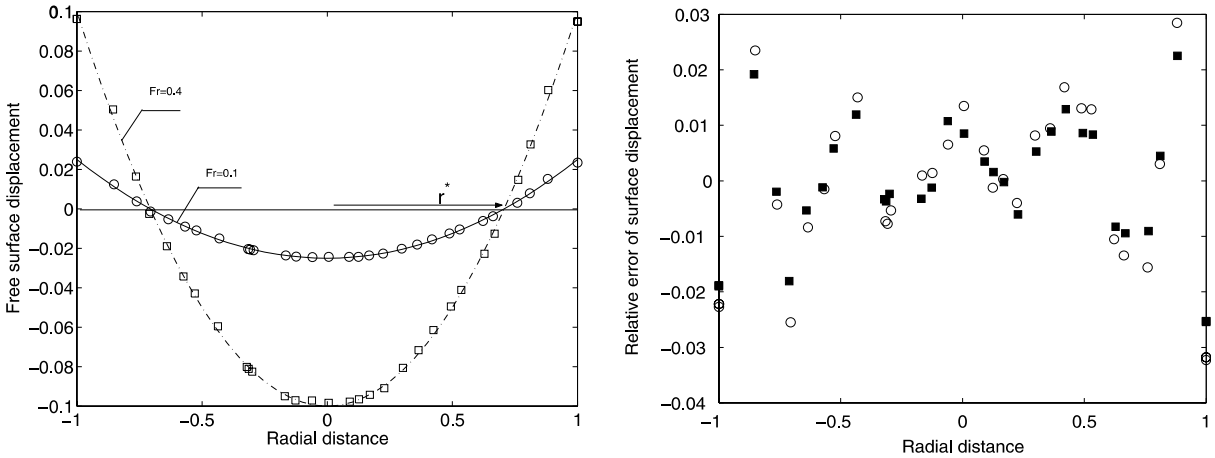

Fig. 14. Left: Computed and analytical free surface shape at $z = 0$ plane for a rotating bucket flow with a constant volume at different Froude numbers; symbols denote computed shapes and solid lines denote analytical shapes. Right: relative errors, open circles denote $Fr = 0.1$ and solid squares denote $Fr = 0.4$.

numerical solutions match the analytical solutions to within 3.2% when $Fr = 0.1$ and 2.5% when $Fr = 0.4$; this example validates the isochoric domain deformation method.

6. Horse-shoe problem

The constraint of local incompressibility may yield mapping equations that cannot describe large deformation. To test whether the incompressible domain deformation method can accommodate large domain deformations, the mapping of a rectangular domain into a curved one is examined here (Fig. 15a and b). This is the so-called horse-shoe problem that is found in Refs. [1,3,5].

Fig. 16 shows the deformation. The domain is deformed progressively by using a (zeroth-order) continuation (or homotopy); each shape is computed by prescribing the location of the narrow boundaries of the "deformed" shape and using the previous shape in the sequence as (unstressed) reference domain. The mesh quality is good at each step of the domain deformation. The use of continuation is not a barrier to adopting

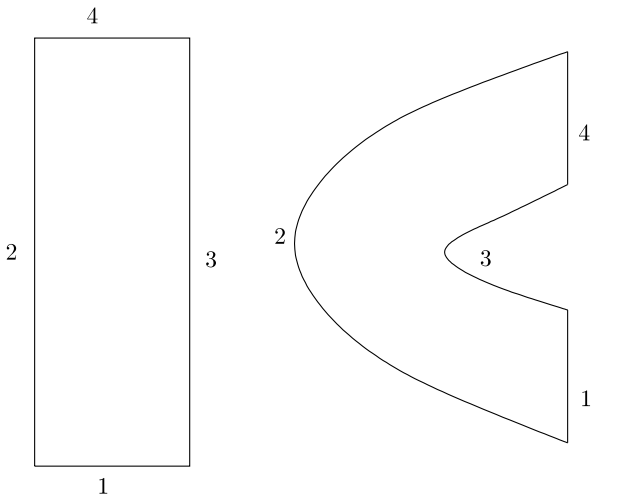

a. Initial rectangular domain b. Deformed horse shoe domain

Fig. 15. Schematic of a rectangle deforming to a horse-shoe shape.

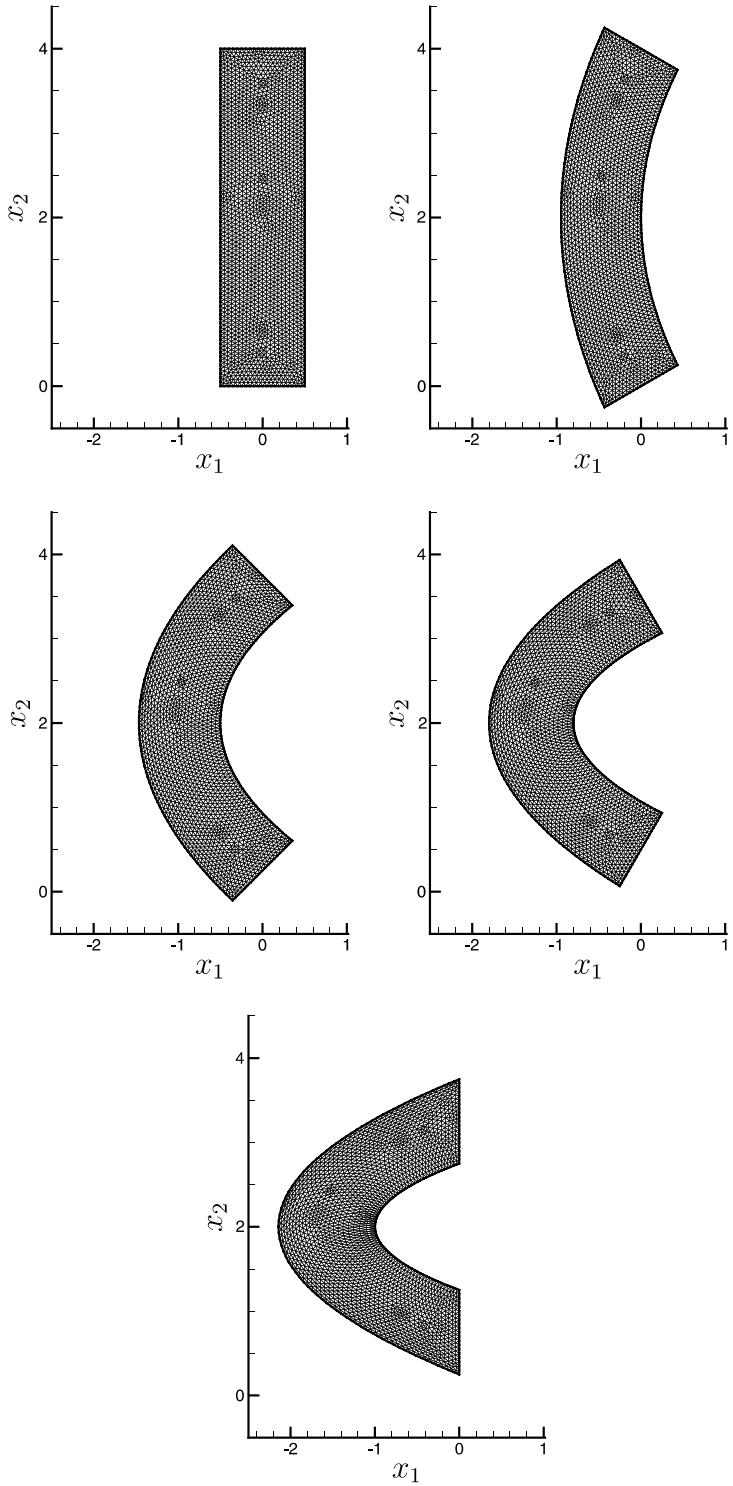

Fig. 16. Meshes of the rectangular domain and its progressively deformed shapes into a horse-shoe.

the incompressible domain deformation method in free surface flow computations because continuation is used routinely in such computations to accelerate the convergence of Newton's method as well as to find turning points and construct bifurcation diagrams [3,8,14–16].

7. Conclusions

A new isochoric domain deformation method is developed in this study. This new method treats a volume-conserved free surface flow domain as an incompressible elastic pseudo-solid. The flow domain is then computed by solving the momentum-conservation equation of the incompressible elastic pseudo-solid together with its volume conservation equation. The equations for fluid and pseudo-solid are coupled to determine flow field and unknown domain simultaneously. The isochoric domain deformation method is an extension of the classical domain deformation method. The key developments in the new method are (1) it treats mesh as incompressible elastic pseudo-solid instead of a compressible one in the original domain deformation method, (2) it replaces one mass conservation equation in the fluid with the specification of a reference value for the mapping pseudo-pressure π to break the linear dependence in the equation set and to form a well-posed system of equations. This new method can be used to compute steady free surface flows with prescribed domain volume, which cannot be handled as easily by the original domain deformation method. Importantly, the new method does not introduce global constraints in the equation set and yields sparse and substantially diagonal matrices when combined with finite element basis functions.

The isochoric domain deformation method is applied in a 2D static case with free surface deformed by capillary force, a 2D drop deformation in a shear flow, and a 3D flow where free surface is deformed due to inertial and gravitational force. The shape of a liquid between two parallel plates is computed successfully, and the analysis of the results shows that the fluid volume is conserved. The 2D drop deformation is calculated at different capillary number and validated by comparing with results of [19]. A 3D rotating bucket with a constant volume of liquid inside is modeled at two different Froude numbers. The free surface shapes match the analytical solutions. Moreover, the incompressible domain deformation method can describe successfully the large nonlinear deformation of a rectangular strip into a horse-shoe shape. Therefore, the isochoric domain deformation method can be used successfully to compute both 2D and 3D, steady, volume-conserved free surface flows.

Acknowledgements

This work was supported by the National Science Foundation under award CTS-ITR-0312764. Computational resources were provided by the Rice Terascale Cluster funded by NSF (EIA-0216467), Intel, and Hewlett–Packard, and the Rice Cray XD1 Research Cluster funded by NSF (CNS-0421109), AMD, and Cray.

Sandia is a multiprogram laboratory operated by Sandia Corporation, a Lockheed-Martin Company, for the United States Department of Energy under contract DE-AC04-94AL85000.

References

[1] V. F. de Almeida, Gas–liquid counterflow through constricted passages, Ph.D. thesis, University of Minnesota, Minneapolis, MN, 1995.
[2] P.A. Sackinger, P.R. Schunk, R.R. Rao, A Newton–Raphson pseudo-solid domain mapping technique for free and moving boundary problems: a finite element implementation, J. Comput. Phys. 125 (1996) 83–103.
[3] L.C. Musson, Two-layer slot coating, Ph.D. thesis, University of Minnesota, Minneapolis, MN, 2001.
[4] K.N. Christodoulou, L.E. Scriven, Discretization of free surface flows and other moving boundary problems, J. Comput. Phys. 99 (1992) 39–55.
[5] V.F. de Almeida, Domain deformation mapping: Application to variational mesh generation, SIAM J. Sci. Comput. 20 (1999) 1252–1275.
[6] M.S. Carvalho, Roll coating flows in rigid and deformable gaps, Ph.D. thesis, University of Minnesota, Minneapolis, MN, 1996.
[7] M. Pasquali, Polymer molecules in free surface coating flows, Ph.D. thesis, University of Minnesota, Minneapolis, MN, 2000.
[8] M. Pasquali, L.E. Scriven, Free surface flows of polymer solutions with models based on the conformation tensor, J. Non-Newtonian Fluid Mech. 108 (2002) 363–409.
[9] R.A. Cairncross, P.R. Schunk, T.A. Baer, R.R. Rao, P.A. Sackinger, A finite element method for free surface flows of incompressible fluids in three dimensions. Part I. Boundary fitted mesh motion, Int. J. Num. Methods Fluids 33 (2000) 375–403.
[10] X. Xie, M. Pasquali, Computing 3D free surface viscoelastic flows, in: A.A. Mammoli, C.A. Brebbia (Eds.), Moving Boundaries VII: Computational Modeling of Free and Moving Boundary Problems, WIT Press, Southampton, UK, 2003, pp. 225–234.
[11] X. Xie, Modeling viscoelastic free surface and interface flows, with applications to the deformation of droplets and blood cells, Ph.D. thesis, Rice University, Houston, TX, 2006.

[12] R. Bouffanais, M.O. Deville, Mesh update techniques for free-surface flow solvers using spectral element method, J. Sci. Comput. 27 (2006) 137–149.
[13] G.A. Holzapfel, Nonlinear Solid Mechanics, first ed., John Woley & Sons, LTD, Chichester, 2000.
[14] S.F. Kistler, L.E. Scriven, Coating flows, in: J.R.A. Pearson, S.M. Richardson (Eds.), Computational Analysis of Polymer Processing, Applied Science Publishers, London, 1983, pp. 243–299.
[15] S.F. Kistler, L.E. Scriven, Coating flow theory by finite element and asymptotic analysis of the Navier–Stokes system, Int. J. Numer. Methods Fluid. 4 (1984) 207–229.
[16] J.H. Bolstad, H.B. Keller, A multigrid continuation method for elliptic problems with folds, SIAM J. Sci. Stat. Comput. 7 (1985) 1081–1104.
[17] L.E. Malvern, Introduction to the Mechanics of a Continuous Medium, first ed., Prentice-Hall, Englewood Cliffs, NJ, 1969.
[18] I.S. Duff, A.M. Erisman, J.K. Reid, Direct Methods for Sparse Matrices, first ed., Oxford University Press, Oxford, 1986.
[19] H. Zhou, C. Pozrikidis, The flow of suspensions in channels: single files of drops, Phys. Fluids A 5 (1993) 311–324.